Appl. Phys. A (2014) 114:51–55
DOI 10.1007/s00339-013-8088-2

Applied Physics A
Materials Science & Processing

INVITED PAPER

Laser nanoablation of graphite

V. D. Frolov · P. A. Pivovarov · E. V. Zavedeeev · M. S. Komlenok · V. V. Kononenko · V. I. Konov

Received: 12 September 2013 / Accepted: 15 October 2013 / Published online: 18 December 2013
© Springer-Verlag Berlin Heidelberg 2013

Abstract Experimental data on laser ablation of highly oriented pyrolitic graphite by nanosecond pulsed UV ($\lambda = 193$ nm) and green ($\lambda = 532$ nm) lasers are presented. It was found that below graphite vaporization threshold ≈ 1 J/cm^2, the nanoablation regime can be realized with material removal rates as low as 10^{-3} nm/pulse. The difference between physical (vaporization) and physical–chemical (heating + oxidation) ablation regimes is discussed. Special attention is paid to the influence of laser fluence and pulse number on ablation kinetics. Possibility of laser-induced graphite surface nanostructuring has been demonstrated. Combination of tightly focused laser beam and sharp tip of scanning probe microscope was applied to improve material nanoablation.

1 Introduction

It has been proved experimentally that short-pulsed laser can be an effective tool for ultra-precision surface nanostructuring of diamond and diamond-like films (see, e.g. [1]). For sufficiently low laser fluence, a quantity of carbon material removed by each repetitive pulse action can be only few clusters or even atoms. Observed average ablation rate was around 10^{-3}–10^{-4} nm/pulse and there is no physical restriction to diminish it. That is why such a regime was called nanoablation [2]. The effect was attributed to laser-induced surface graphitization and further oxidation of carbon material. At higher laser fluence, graphitic material vaporization starts. In this case, depending on laser pulse duration and intensity, the ablation rate is typically in the range 10^2–10^5 nm/pulse.

The primary aim of this work was investigation of laser ablation of graphite which is interesting not only from the point of view of modeling of laser nanoablation of diamond materials. Of particular importance is also to find new ways to laser nanoablation and nanostructuring of graphene. The obtained data on graphite can be applied, e.g. for controlled local removal of single or several graphene layers.

Another part of our work was investigation of graphite nanoablation by combined action of the focused laser beam and the cantilever tip of the scanning probe microscope (SPM). On one hand, it is well known that near the subwavelength surface structures or objects, such as the sharp probe tip, strong laser field enhancement occurs [3]. This effect is used, e.g. in tip-enhanced Raman spectroscopy [4]. On the other hand, it was found that under combined thermochemical (by applied electrical pulses) and mechanical action of the probe, ultra precise (10^{-3}–10^{-2} nm/pulse) nanoablation of graphite and graphene sheets can be induced [5,6]. In this case, besides ultra high vertical resolution, spatial resolution of about 10 nm for the produced structures was demonstrated.

Meanwhile, we have failed to find publications on graphene-based materials nanostructuring by means of laser and SPM combination.

2 Experimental details

The samples of highly oriented pyrolitic graphite (HOPG) were used in this study, and all experiments were performed in air environment.

In the first series of experiments, only laser irradiation was carried out. Excimer ArF-laser (Laser 1) beam had the wavelength $\lambda = 193$ nm, pulse duration $\tau = 20$ ns and pulse

V. D. Frolov · P. A. Pivovarov · E. V. Zavedeeev · M. S. Komlenok · V. V. Kononenko · V. I. Konov (✉)
A. M. Prokhorov General Physics Institute of RAS, 38 Vavilov str., Moscow 199991, Russia
e-mail: konov@nsc.gpi.ru

repetition rate $f = 50$ Hz and was projected into 45×45 μm^2 square spot on the graphite sample. The laser pulse fluence E was varied from 0.25 to 7 J/cm^2. The depth D of the crater, produced by N laser pulses, was measured by the interferometer "Zygo" and thus average ablation rate $V = D/N$ [nm/pulse] can be determined.

In the second series, the sample was placed inside the SPM "Integra Spectra M" (Fig. 1).

As an SPM probe, special highly conductive n-type silicon cantilever with the tip radii ≈10 nm was used. It operated in a tapping mode at resonant frequency about f_t ≈300 kHz. The amplitude of cantilever oscillations did not exceed 100 nm. A sharp nose form of the probe tip allows one to focus the beam of a pilot laser (Laser 2) below the end of the probe tip with minor energy losses. Laser 2 had the following features: $\lambda = 532$ nm, $\tau = 7$ ns, pulse repetition rate = 0.1–2.5 kHz. The focal spot diameter on the sample surface was about 1 μm; laser fluence was varied in the range 0.1–10 J/cm^2. To determine laser ablation rate with or without the probe tip, the difference in surface relief maps, controlled by scanning SPM probe before and immediately after laser treatment, was evaluated.

It is important to point out that because of relatively low pulse repetition rate $f \leq 2.5$ kHz, the absorbed laser energy between laser pulses is spread outside irradiation spot for both series. It means that heat accumulation effects can be neglected. Really, thermal diffusivity along graphene sheets in graphite is $\chi_{II} \approx 12$ cm^2/s. The length of heat spreading between laser pulses is $L_{II} \approx (\chi_{II}/f)^{1/2} \gg 100$ μm and, correspondingly, much more than spot diameters for both lasers. In graphite, for the used laser wavelengths, light penetration into the material is about $\ell \approx 10^{-6}$cm; while during each laser pulse action, heat penetration length into the sample is $L_\perp \approx (\chi_\perp \tau)^{1/2}$, where $\chi_\perp \approx 2$ cm^2/s is the heat diffusivity in the direction normal to graphene layers. For laser pulses used in our experiments ($\tau \sim 10^{-8}$ s), we have $L_\perp \approx 10^{-4}$ cm $\gg \ell$. So, taking into account that graphite reflectivity is weakly dependent on λ and $L_\perp \sim \tau^{1/2}$, we should expect that surface temperature and thermal thresholds should be close for both lasers.

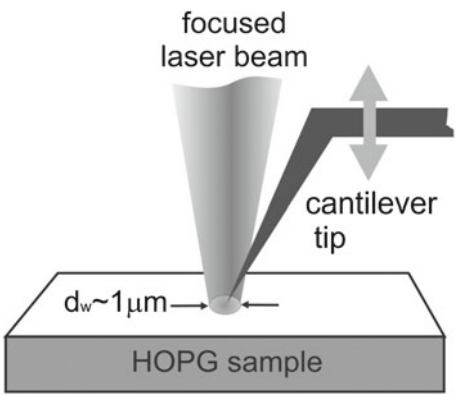

Fig. 1 The scheme of laser–probe ablation in SPM

3 Experimental results and discussion

3.1 UV laser irradiation

The ablation rate dependence on ArF-laser fluence is shown in Fig. 2. For each E, we took the data on the maximal V value which for small fluences was obtained during the initial pulse train ($N \leq 10^2$–10^3) and for high E did not depend on pulse number. For comparison, $V(E)$ data related to the first pulses of green laser (see Fig. 3) is presented (open triangles).

One can see that ablation rate for small E can be as low as 10^{-3}–10^{-2} nm/pulse. It means that much less than a monolayer (graphene sheet thickness is ≈0.3 nm) can be removed on average by each laser pulse. Similar nanoablation regime was observed for diamond materials. We believe that multiple laser pulse action leads to formation of defects in graphene structure and removal of weakly bonded atoms via thermal oxidation. This mechanism looks similar to diamond nanoablation when local graphitization (formation of carbon nanoclusters) and its further oxidation are considered.

Growth of laser fluence leads to increase in ablation rate. We found that there are two different regions of $V(E)$ dependence. For $E < E_a \approx 1$ J/cm^2, we have very fast growth of ablation rate with laser fluence ($V \infty E^k$, $k = 5$–10). While $E > E_a$, the ablation rate grows practically linear with E. Such a dependence is typical for material surface vaporization ablation with the threshold E_a and is characterized by relatively high ablation rate ($V \geq 10$ nm/pulse).

3.2 Green laser irradiation

The important feature of this series is the dependence of the ablation rate V on the pulse number N. Both below and above

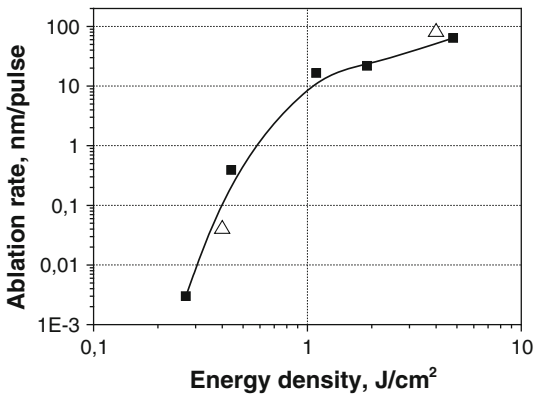

Fig. 2 The ablation rate v.s. pulse energy density plots in the case of UV laser irradiation (*solid squares*). *Open triangles* relate to $V(E)$ data for green laser

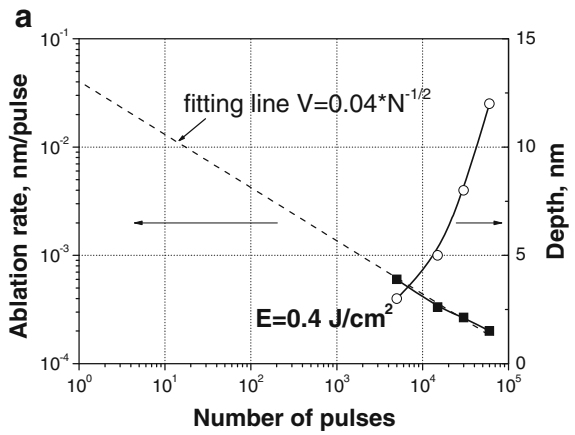

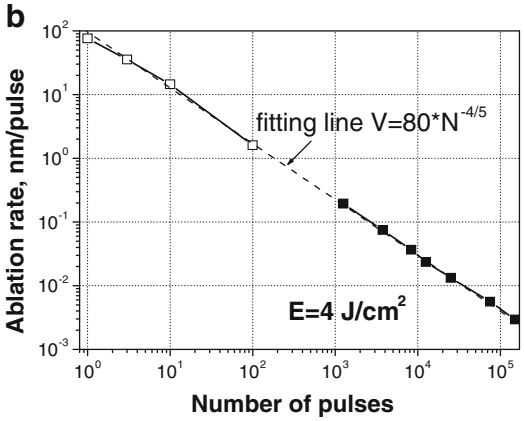

Fig. 3 The ablation rate (left scale) v.s. pulse number plots: **a** below the threshold ($E = 0.4$ J/cm^2), **b** above the threshold ($E = 4$ J/cm^2). In addition, the crater depth (see (**a**), right scale) v.s. pulse number plot is shown. In (**b**), $V(N)$ data obtained for single pulse trains and pulse repetition rate ($f = 1.5$ kHz) regimes are shown by *open* and *solid squares*, respectively

vaporization ablation threshold ($E_a \approx 1$ J/cm^2, close to the value measured for the UV laser), the ablation rate $V = D/N$ decreases with increasing N (see Fig. 3).

In addition, the $D(N)$ dependence is shown in Fig. 3a. The experimental data on $D(N)$ are registered only at $N \geq 4 \times 10^3$ pulses ($D \geq 3$ nm) because the depth detectivity is limited by the sample roughness of 2–5 nm. If we take the highest V values that correspond to the first laser pulses, we see that both the point $V = 0.04$ nm/pulse, estimated by fitting the experimental curve $V(N)$ for $E = 0.4$ J/cm^2 (Fig. 3a), and the point $V = 80$ nm/pulse for $E = 4$ J/cm^2 (Fig. 3b) are well matched with the curve $V(E)$ obtained with Laser 1 (see Fig. 2).

To our opinion, there are two different mechanisms responsible for ablation rate variation with laser pulse number. It is noteworthy that both of them result from structural modification of graphite layers under prolonged laser irradiation. We believe that fundamental mechanism of graphite nanoablation is determined by existing (prior to irradiation) and laser produced defects in the upper oxidized graphene sheet. Apart from that, the laser treatment can lead to both ordering and disordering in carbon-based systems. The key factor is the value of temperature induced by laser heating. On one hand, it can be high enough to move graphite into amorphous form. As is always the case, when material density falls, the matter expands and irradiated surface swells. This process could be long enough and captures deeper graphite layers from pulse to pulse. The competition between laser-induced etching of surface and its swelling can cause specific non-linear dependence $D(N)$. On the other hand, if laser heating is not so high to produce the allotropic transformation it can assist the annealing of HOPG, reducing gradually the number of pre-existing ("as received") defects. Then, the efficiency of graphite sheet oxidation will decrease from pulse to pulse and $D(N)$ curve should saturate. For graphite vaporization, the surface temperature T_s should exceed $T_v \approx 4,000$ K, so for $E = 0.4$ J/cm^2 we have $t_s = T_v(E/E_a) \approx 1,600$ K. For better understanding, careful investigation of the structure of laser irradiated graphite should be done.

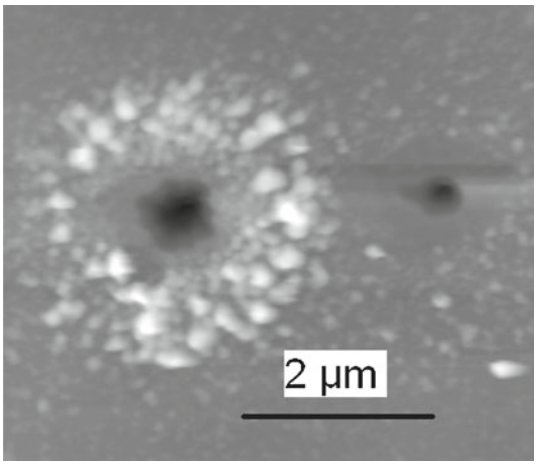

Fig. 4 The sample surface after laser actions far away the probe (*right*) and at the probe-sample contact region (*left*). The number of laser pulses is $N = 6 \times 10^4$, the laser energy density is $E = 4$ J/cm^2

Above the graphite vaporization threshold, ablation rates are so high that during a few initial laser shots quite a deep crater is formed in the irradiated zone. For instance, after only 10 laser pulses at $E = 4$ J/cm^2, the crater depth D is more than 150 nm and becomes comparable with the crater radius. For this experiment the Rayleigh length is only about 1.5 μm, the crater walls are highly absorbing and one can expect strong energy losses, especially in deep craters. Figure 4 (right spot) demonstrates the SPM image of the crater produced by $N = 6 \times 10^4$ laser pulses, and Fig. 5 (gray curve) shows the measured cross-section of the crater.

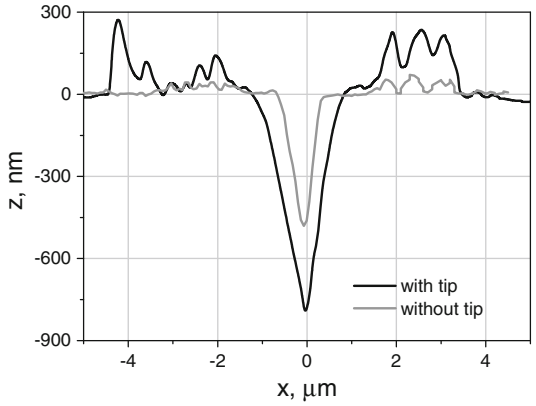

Fig. 5 The surface profiles along the line made across the craters: laser–probe ablation (*black curve*); solely laser ablation (*gray curve*). $N = 6 \times 10^4$, $E = 4$ J/cm^2

One can see that the crater has a conical shape and its depth is about half micron that is comparable with D value after few laser shots. Such an ablation behavior is typical for microhole drilling when, after deep penetration into the solid body, the ablation process is practically stopped because only small portion of laser pulse energy reaches the crater bottom. We also can not entirely exclude minor errors in crater profile measurement by SPM probe. Nevertheless, control experiments with a test object (a grating with 0.5 μm deep grooves, 1.5 μm width and flat bottom) have shown high precision of our technique.

Another important factor that influences ablation process is laser- produced plasma in graphite target vapor plume. At $E > E_a$, beam intensity is about 10^8 W/cm^2 that is quite sufficient to produce such plasmas which were observed in our experiments with Laser 2 (not with Laser 1). According to numerous experiments with nanosecond lasers, plasmas in vapor plumes of various materials can absorb essential part of laser pulse energy [7,8]. The plasma screening effect is strongly influenced by plasma radial expansion. For the considered case, plasma temperature can be roughly estimated as 10^4K and its front should move with $w \sim 10^5$ cm/s velocity. During laser pulse action τ plasma region diameter will reach about $d_p \approx w\tau \approx 10\mu$m. So, plasma cooling by radial expansion is important for the beam with 1 μm diameter. In deep enough craters, the walls will confine plasma, increase its temperature at later stages and absorption of laser pulse. As a result ablation rate inside craters, produced by multi-pulsed irradiation, should be smaller than at a flat surface. Such plasma formation effect should be especially important for the IR laser radiation and can be neglected for the UV pulses.

Note, that some debris are formed outside the crater, see Fig. 4 (right) and Fig. 5 (black curve). That is usual for vaporization ablation regime when hot carbon atoms are expelled into ambient atmosphere, condense and redeposit outside the crater.

We expect that laser nanoablation can become an efficient way to produce shallow structures on the graphite surface, or be used for removal of single or several graphene layers. As an example, Fig. 6 demonstrates the 4×4 μm^2 squared, 150 nm deep crater formed in HOPG by scanning the focused laser beam ($E = 0.7$ J/cm^2, $N = 10^6$ pulses). The crater bottom roughness is of 0.5 nm.

3.3 Laser–probe combination

The comparison of graphite ablation by solely Laser 2 and its combination with the SPM probe is given in Fig. 7.

One can see that the crater depth D is equal in both cases for nanoablation regime ($E \leq E_a$), but ablation rate for the combination is higher when graphite vaporization takes place ($E \geq 1 - 2$ J/cm^2). The crater profile becomes sharper and deeper (Fig. 5, black curve). At the same time, the crater diameter slightly increases. The size and concentration of the redeposited carbon particles around the crater also grow (Fig. 4, left). All these facts definitely evidence that addition of SPM probe can essentially enhance the productivity of graphite vaporization ablation process.

We consider that this effect (and its absence in nanoablation regime) is a result of the SPM feedback response which keeps constant the distance between the probe tip and the sample surface. In the process of crater deepening by laser ablation, this condition is fulfilled by moving the sample in

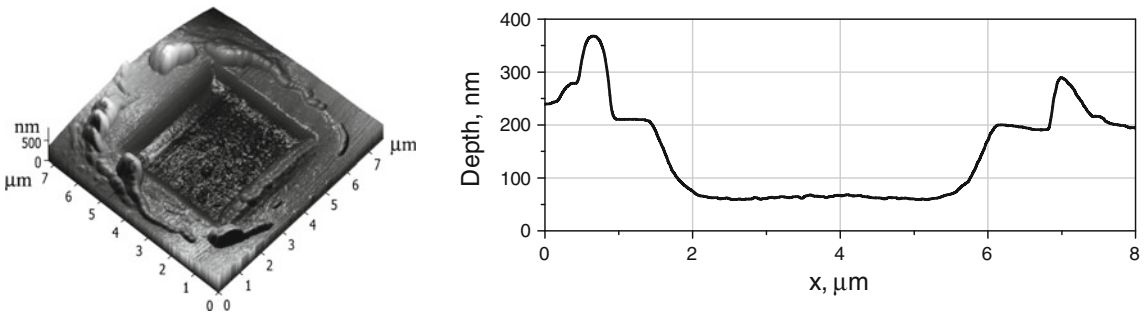

Fig. 6 The 4×4 μm^2 squared crater in graphite: isometric view (*left*); the crater cross-section (*right*)

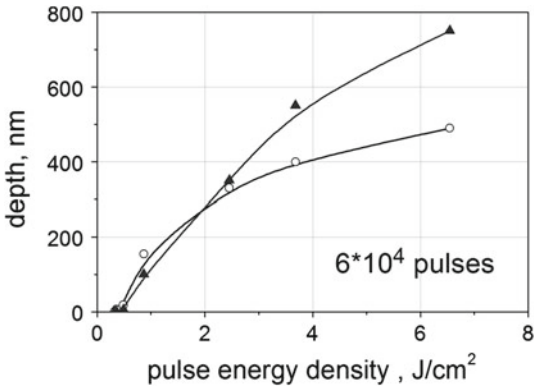

Fig. 7 Comparative $D-E$ plots for solely laser (*opened circles*) and laser–probe (*solid triangles*) ablations

the direction of the laser. Correspondingly, the focal plane of the lens moves down into the crater and thus higher laser intensity at the bottom can be achieved in comparison with solely laser action on a static sample.

4 Conclusions

It has been shown that laser nanoablation of graphite with ultra-small rates $\geq 10^{-3}$ nm/pulse can be realized. This effect has great potential for surface nanostructuring of graphite and graphene. It is found that addition to a laser of the tip of SPM can enhance formation of microholes by laser ablation.

Acknowledgments The work is supported by MES of Russia grant 2012-1.2.1-12-000-2013-061, RFBR grant # 12-02-01167 and RAS Program #24.

References

1. Vitaly I. Konov, Laser in micro and nanoprocessing of diamond materials. Laser Photon. Rev. **6**(6), 739–766 (2012)
2. V.V. Kononenko, M.S. Komlenok, S.M. Pimenov, V.I. Konov, Photoinduced laser etching of a diamond surface. Quantum Electron **37**(11), 1043–1046 (2007)
3. Y. Inouye, P. Verma, T. Ichimura, S. Kawata, in *Tip Enhancement*, ed. by S. Kawata, V. M. Shalaev (Elsevier, Amsterdam, 2007)
4. H. Watanabe, Y. Ishida, N. Hayazawa, Y. Inouye, S. Kawata, Tip-enhanced near-field Raman analysis of tip-pressurized adenine molecule. Phys. Rev. B Condens. Matter Mater. Phys. 2004, **69**(15), p. 155418 (2004)
5. S.V. Kosheleva, V.D. Frolov, V.I. Konov, SPM bipolar pulsed nanostructuring of graphitic layers. Appl. Phys. A. doi:10.1007/s00339-012-7120-2
6. V.I. Konov, V.D. Frolov, E.V. Zavedeev, V.V. Kononenko, S.V. Kosheleva, A.A. Khomich, V.G. Pereverzev, A. Grigorenko, K.S. Novoselov, Fabrication of graphene nanostructures by probe nanoablation. Bull. Lebedev Phys. Inst. **39**(12), 330–333 (2012)
7. S.M. Klimentov, S.V. Garnov, T.V. Kononenko, V.I. Konov, P.A. Pivovarov, F. Dausinger, High rate deep channel ablative formation by picosecond-nanosecond combined laser pulses. Appl. Phys. A **69**(Suppl.), S633–S636 (1999)
8. C. Boulmer-Laborgne, J. Hermann, B. Dubreuil, Plasma formation resulting from the interaction of a laser beam with a solid metal target in an ambient gas. Plasma Sour. Sci. Technol. **2**, 219–226 (1993)